Journal of Colloid and Interface Science 470 (2016) 204–210

Contents lists available at ScienceDirect

Journal of Colloid and Interface Science

journal homepage: www.elsevier.com/locate/jcis

Simple and versatile one-step synthesis of FeS_2 nanoparticles by ultrasonic irradiation

M. Khabbaz [a,c], M.H. Entezari [a,b,*]

[a] Sonochemical Research Center, Department of Chemistry, Faculty of Science, Ferdowsi University of Mashhad, 91779 Mashhad, Iran
[b] Environmental Chemistry Research Center, Department of Chemistry, Faculty of Science, Ferdowsi University of Mashhad, 91779 Mashhad, Iran
[c] International Campus, Ferdowsi University of Mashhad, Mashhad, Iran

GRAPHICAL ABSTRACT

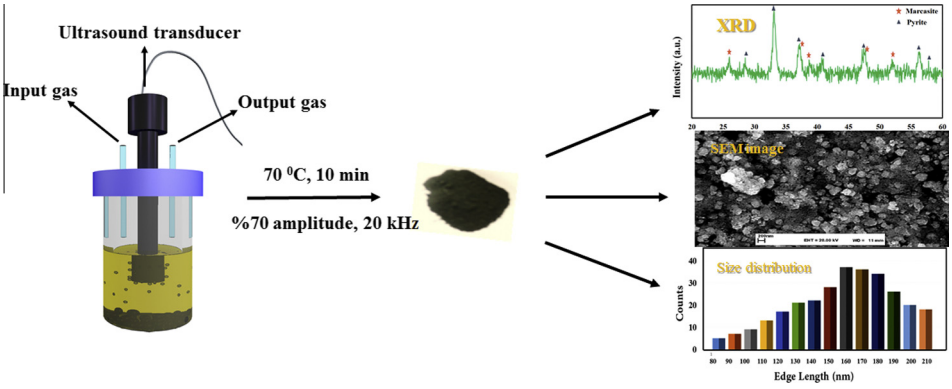

ARTICLE INFO

Article history:
Received 6 January 2016
Revised 23 February 2016
Accepted 23 February 2016
Available online 24 February 2016

Keywords:
Pyrite
Synthesis
Ultrasound
Nanoparticle

ABSTRACT

The synthesis of stable pyrite nanocrystals (NCs) in a simple way is very difficult. A facile and single-stage ultrasonic synthesis route has been successfully developed for the preparation of pyrite (FeS_2) NCs in 10 min and 70 °C. In this study, the influences of reaction time, temperature, and acoustic power on the formation of the target compound were considered. In addition, a comparison was made of the synthesis of pyrite NCs by sonication with 20 kHz apparatus and by the classical method (without ultrasound). The as-prepared pyrite was characterized by X-ray diffraction (XRD), Fourier transform infrared (FT-IR), scanning electron microscopy (SEM), Raman spectrophotometry and energy-dispersive X-ray spectroscopy (EDS). The XRD of the sample prepared by classical method indicated a typical cubic FeS_2 with space group *Pa*3 and the average size of 16 nm. Sulfur as an impurity in the sample was verified by XRD analysis. The sample prepared by ultrasound showed two phases of pyrite, cubic and marcasite structures. The space groups were *pa*3 and pnnm, respectively and the average size was 28.8 nm. According to the SEM images, the morphology of the synthesized pyrite using the two methods are closely the same. The FT-IR and Raman spectra presented the Fe═S, Fe—S and S—S functional groups. In addition, the sono-synthesis of pyrite was done under milder conditions and in shorter time with better features than classical method.

* Corresponding author at: Sonochemical Research Center, Environmental Chemistry Research Center, Department of Chemistry, Faculty of Science, Ferdowsi University of Mashhad, 91779 Mashhad, Iran.
E-mail addresses: entezari@um.ac.ir, moh_entezari@yahoo.com (M.H. Entezari).

http://dx.doi.org/10.1016/j.jcis.2016.02.055
0021-9797/

1. Introduction

With the growing necessity of the high-quality mineral materials, interest has been focused on the synthesis of nano scaled mineral compounds with controlled growth, structure and size [1]. There are several types of iron sulfides in nature i.e. FeS_2 (pyrite and marcasite), Fe_3S_4 (greigite) and $Fe_{1-x}S$ (pyrrhotite) [2]. Pyrite is slightly oxidized relative to other metal sulfide minerals, because it is so abundant on the earth [3]. Also, pyrite has extreme applications and can be used in different industries. FeS_2 as a semiconductor has a narrow band gap, high light absorption coefficient, and excellent properties in photoelectric conversion [3–6]. It is widely used in solar photoelectric materials and in high energy density batteries fields [7,8]. Pyrite particles were also used in catalytic processes for degradation of some resistant pollutants [9]. Pyrite can produce sufficient OH radical to footprint DNA in biological processes [10]. Up to now there is one concern for fabricating pyrite nanoparticles by a simple method. So far, FeS_2 crystals and films were made by various techniques. Several routes for the synthesis of micro and nano iron sulfide material such as ball milling [11], mechanochemical [12], magnetron sputtering [13], heating up [14,15], microwave synthesis [1], solvothermal method with surfactant-assisted-mediated [6,15–19] or without surfactant [4,20–22], hydrothermal [18,23–25], electrochemical deposition [26], chemical bath deposition [4,27] had been reported. However, studies on the synthesis of FeS_2 nanoparticles were rather sparse. In all methods, it has been tried to form one uniform and appropriate product at low temperature and short time. As yet many studies have been taken on the synthesis of pyrite nanoparticles, unfortunately, the approaches applied used considerable time and high temperatures [28–31]. In addition, the synthesis method and the products obtained essentially depended on the precursor and setup of the system because sometimes there are impurities in the products (Fe—S compounds) which greatly hinder their performance [16]. Some of methods cannot produce pyrite in a single stage process so that they require excess sulfur to convert other phases such as FeS or FeS_{2-x} into pyrite [32].

Synthesized pyrite nanoparticles were made in different shapes and structures such as cubic [14,20], octahedral [16], nanoflake and microsphere [33], flower [19], nanorod [34] and other shapes. The cubic structure is more stable than other structures [35]. The unit cell of pyrite contains four formula units (FeS_2). The Fe^{2+} cations are located in a face-centered cubic sub lattice, and the $(S_2)^{2-}$ dimers are placed at the centers of the cubic edges and the structure is almost the same as unit cell of NaCl [36,37].

In spite of abundant pyrite in nature, its synthesis is necessary, because natural pyrite is not pure and the impurity affects its different applications. Previous methods in the synthesis of pyrite used long times and high temperatures, consequently, there is a need to design a fast and reliable synthesis route for the pyrite nanoparticles. Ultrasonic irradiation is an efficient technique for the synthesis of many materials. Chemical effects of ultrasound are the result of indirect interaction between the sound waves and molecules, because the sound wavelength is considerably longer than the size of the molecule. Chemical effects of ultrasound can be derived by acoustic cavitation which includes formation, growth and implosive collapse. Transient collapse generates high temperatures (~5000 K) and high pressures (about 1000 atmosphere). For these reasons, it seems that ultrasound method can be an efficient way for the synthesis of pyrite nanoparticles [38]. In this research, the synthesis of iron sulfide was carried out through sonication of a system which was sealed completely. Ultrasonic irradiation is one of this paper's innovations that leads to increase the mass transfer, high temperature and pressure during the cavitation process. These conditions not only reduced the time but also reduced considerably the temperature of reaction. It should be mentioned that ultrasound has emerged as a versatile technique for producing nanostructures with suitable size and morphology. Besides, the product synthesized using classic method (PC) was compared with the sample synthesized under ultrasound (PU). In this comparison, the main advantages of the ultrasonic method are due to short reaction time, low processing temperature, high purity and uniform shapes. One of the most challenging issues is to control pure products with defined morphology and our approach can fulfill this aim. Finally, our methodology is single-stage and does not require expensive source precursors or toxic solvents and the morphologies of the products are well controlled. In addition, designated raw materials lead to produce more appropriate and stable structure of the nanoparticles.

2. Experimental procedures

Details of experiments, comparing of ultrasound and classical methods in synthesis, and characterization techniques were utilized for synthesized pyrite NCs in both ways.

2.1. Materials

Iron (II) sulfate heptahydrate ($FeSO_4{\cdot}7H_2O$), Sodium thiosulfate pentahydrate ($Na_2S_2O_3{\cdot}5H_2O$), absolute ethanol that all were obtained from Merck company. All reagents were of analytical grade and were used without further purification. In addition, distilled water and ethanol were used for washing. Argon gas was employed to eliminate air or oxygen from the reaction flask.

2.2. Methods

2.2.1. Classic method

In a typical conventional process, 2.68 g $FeSO_4{\cdot}7H_2O$, 6.68 g $Na_2S_2O_3{\cdot}5H_2O$ with 100 ml absolute ethanol were poured into in a three-neck flask and then it was sparged under Argon atmosphere to remove air. The molar ratio of sulfur to iron was about 6:1. The reflux system was sealed and the mixture was stirred by magnetic stirrer, then the temperature of the suspension was maintained about 200 °C for a period of 24 h. Afterward the precipitate produced was cooled to room temperature naturally. The dark precipitates were washed and were centrifuged sequentially with distilled water and ethanol to remove the residual impurities. Subsequently the product was dried at 80 °C for 4 h in a vacuum oven. Then the dark powder was collected and take placed within vial into a desiccator for characterization.

2.2.2. Ultrasonic method

The ultrasound approach was carried out with same amount of initial materials used in the classic method. After addition of initial materials, the cell was sealed and put 15 min under Argon atmosphere and then the reaction was carried out under ultrasound at 70 °C for 10 min. After that the reaction product was cooled to room temperature gradually while it was still in a sealed cell. The pH of suspension was inherent pH of the mixture and it reached to 5.9 after reaction. The dark precipitates were washed and were centrifuged consecutively with distilled water and ethanol to take away the remaining impurities. In spite of pyrite oxidation is not very fast, the dark precipitates were placed into a closed Erlenmeyer and were washed fast. Then the samples were dried at 80 °C for 4 h in a vacuum oven and finally the dark powders were gathered in vial within desiccator for characterizing. Difference of

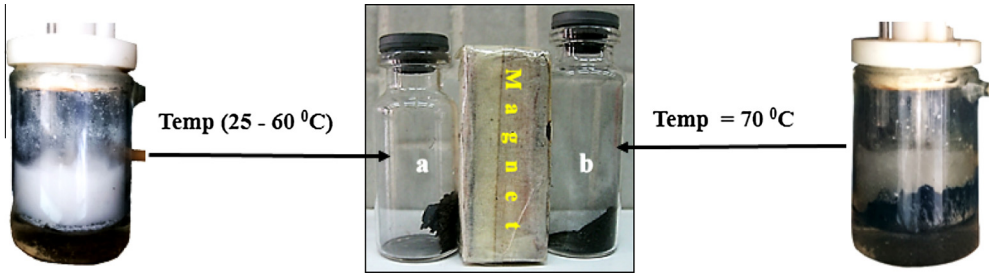

Fig. 1. Product comparison in condition of (a) less than 70 °C and (b) equal to 70 °C during the reaction conditions (10 min ultrasound irradiation, 70% electrical power).

two methods was in the magnitude of time and temperature of reaction.

2.3. Characterization and instrument

Ultrasonic waves were irradiated using XL2020 model instrument with 550 W electrical power and 20 kHz frequency. XRD patterns were collected with a Bruker-axs, D8 Advance model at a scanning rate of 0.05°/s, using monochromatized Cu Kα radiation (k = 1.5406 Å) and a wide range angle (2θ° = 20–60). The patterns were collected using a 0.04° step–scanning mode. The morphology and particle size of the yields were investigated by SEM model Leo 1450VP from LEO Germany Company with magnification 20–300,000 times and equipped with EDX detector, also TEM model Philips CM120 120 kV. Raman spectroscopy was performed with an Almega Thermo Nicolet Dispersive Raman spectrometer with a 1064 nm laser wavelength, exposure time 13,000 ms and laser power 490 mw. Samples were dispersed in water and then the spectrum was taken. FT-IR spectra were documented on a Thermo Nicolet 370 spectrometer, the spectrum was attained by mixing the sample with KBr and water was removed. The FT-IR and Raman spectra presented the Fe═S, Fe—S and S—S functional groups. EDS was taken on JEM-2100F transmission electron microscopy.

3. Results and discussion

3.1. Pyrite formation

Following processes concisely demonstrate the total synthetic procedures and probable reactions.

It has been assumed that pyrite formation occurs by a four step progression [1,16,32].

$$2Na_2S_2O_3 \cdot 5H_2O \rightarrow 2Na_2SO_3 + 2S + 10H_2O \quad (R\text{-}1)$$

$$2CH_3CH_2OH + 2S \rightarrow 2CH_3CHO + 2S^{2-} + 4H^+ \quad (R\text{-}2)$$

$$FeSO_4 \cdot 7H_2O + S^{2-} \rightarrow FeS + SO_4^{2-} + 7H_2O \quad (R\text{-}3)$$

$$CH_3CHO + FeS + S^{2-} + 2H^+ \rightarrow CH_3CH_2OH + FeS_2 \quad (R\text{-}4)$$

In the first step, sulfur element forms via decomposition of sodium thiosulfate pentahydrate ($Na_2S_2O_3{\cdot}5H_2O$) (R-1). In the second step, the sulfur atom was reduced to S^{2-} by means of ethanol (R-2). In the third step, iron monosulfide (FeS) forms through the reaction between sulfide and ferrous ions in ethanol (R-3). Finally, FeS is transformed to pyrite based on (R-4). The intermediates such as S and FeS were verified by XRD. In addition, magnetic precipitates were formed during the reaction before the end of the reaction (Fig. 1). The main species for the formation of pyrite based on reactions are Fe^{2+} and S° (or S^{2-}). For preventing Fe(II) oxidation as the iron source, the suspension was sparged by Ar gas. In addition, ethanol was considered as a reducing agent and as a dispersant in order to avoid forming iron (II) hydroxide and magnetite precipitation, whereas, if water is used as solvent, iron (II) is oxidized to iron (III), and finally iron (III) hydroxide is formed.

The presence of $FeSO_4{\cdot}7H_2O$, $Na_2S_2O_3{\cdot}5H_2O$ in the heterogeneous system of ethanol can result in the formation of pyrite according to the following overall reaction:

$$FeSO_4 \cdot 7H_2O + 2Na_2S_2O_3 \cdot 5H_2O + C_2H_5OH \rightarrow FeS_2 + 2Na_2SO_3 + H_2SO_4 + CH_3CHO + 11H_2O$$

3.2. Optimum conditions

To evaluate product efficiency, the optimization of reaction under ultrasound has been carried out at different powers, times of sonication, and temperatures. Based on XRD and FTIR analysis, low temperatures and low powers do not lead to a favored product. Besides, distinct irradiation time is necessary to have an anticipated powder. When the sonication was applied from ambient

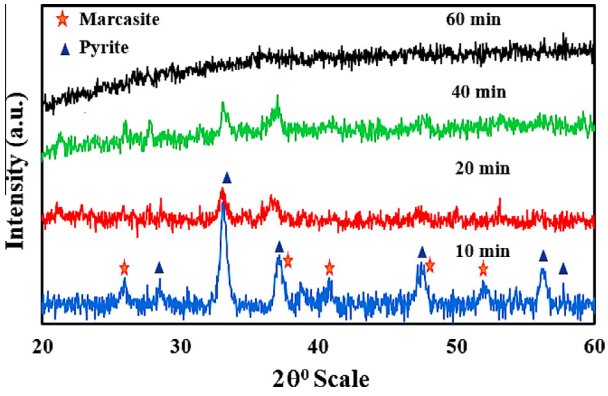

Fig. 2. Comparison of XRD pattern of products in different time by ultrasound method (70 °C, 70% electrical power).

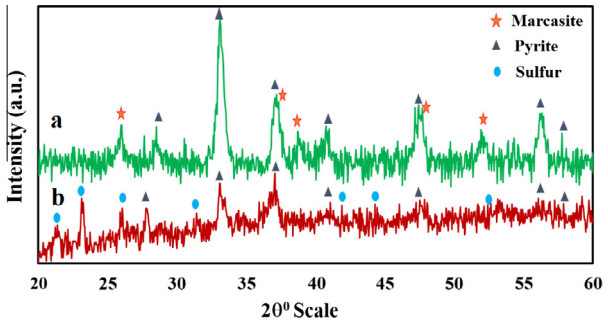

Fig. 3. Pyrite NCs XRD spectra; (a) ultrasound method (10 min ultrasound irradiation, 70 °C, 70% electrical power), (b) classic (24 h heating, 200 °C, reflux).

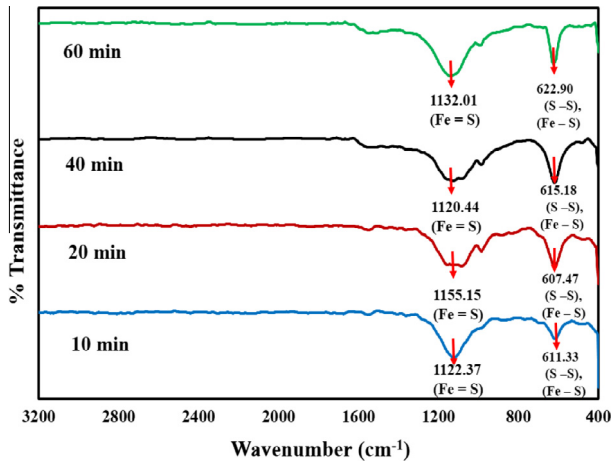

Fig. 4. Comparison of FTIR spectra of PU at different times (70 °C, 70% electrical power).

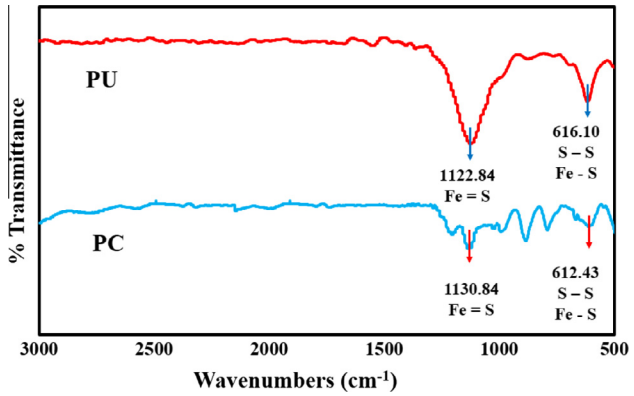

Fig. 5. Comparison of FTIR spectra for PU (10 min ultrasound irradiation, 70 °C, 70% electrical power) and PC (24 h heating, 200 °C, reflux) of products.

temperature with low electrical power, in spite of temperature rising during ultrasonic irradiation, no suitable precipitate was achieved. Pyrite nanoparticle is a black precipitate and is diamagnetic, whereas in preceding conditions a brown solid was formed. However, sometimes a dark precipitate was made but it exhibited magnetic properties as it is shown in Fig. 1 by a simple magnet. In long times of sonication, based on the XRD analysis, the characteristic peaks of pyrite were disappeared. This means that the pyrite is amorphous or has a very small size that cannot be characterized by XRD [39]. The best product was synthesized at 70 °C and sonication at 70% electrical power for 10 min. The black and diamagnetic precipitate was collected and was characterized by different techniques.

3.3. X-ray analysis

Fig. 2 shows the XRD pattern of products which were synthesized in different times of sonication. According to Fig. 2, the crystal phase related to the pyrite vanished with increasing the time of sonication. In an hour of sonication, no peaks were observed in XRD pattern and it seems the powder obtained is in an amorphous state [40]. With decreasing of sonication time, the index peaks of pyrite in XRD appeared and 10 min of sonication was the proper time for crystalizing of pyrite. Fig. 3 shows the XRD patterns for the two samples prepared in the presence and absence of ultrasound. The XRD patterns were perfectly consistent with pyrite phase with exact peak positions and the same relative peak intensities in both samples. It implied that the products synthesized by ultrasound had cubic (pyrite) and orthorhombic (marcasite) phases without distortion and randomly oriented. The lattice parameters for cubic structure is (a = b = c = 5.418 Å) and for orthorhombic is (a = 4.445 Å, b = 5.425 Å, c = 3.388 Å). In ultrasound, other parameters such as d spacing and FWHM were about 2.0–3.9 Å and 0.28–0.46°2Th based on 2θ° = 33.961, respectively. Whereas in the classic method, the parameters mentioned for the cubic phase of pyrite were 2.4–3.8 Å and 0.3–0.7°2Th based on 2θ° = 33.104, respectively. Besides, the lattice parameters of this sample were the same (a = b = c = 5.418 Å). Additionally, from the XRD pattern of the classical sample, some other weak peaks (marked with blue circle on the Fig. 3) were assigned to sulfur as the impurity. In both resulting samples there was no trace of the other iron sulfide phases such as $Fe_{1-x}S$, or FeS. The presence of sharp peaks in the XRD patterns confirmed the highly crystalline nature. The average size of unit cell for the classical and sonochemical pyrite NCs using Debye-Scherer equation were estimated to about 16 and 28.8 nm, correspondingly.

3.4. FTIR analysis

Fig. 4 shows the FTIR spectrum of the FeS_2 nanoparticles that were synthesized by ultrasound in different times. According to FTIR spectra, the characteristic peaks around 1120–1156 cm^{-1} are related to pyrite surface chemistry (Fe═S) [41] and around 607–622 cm^{-1} are related to stretching S—S and Fe—S bonds [11,42–44]. Based on Fig. 4, the functional groups are characterized

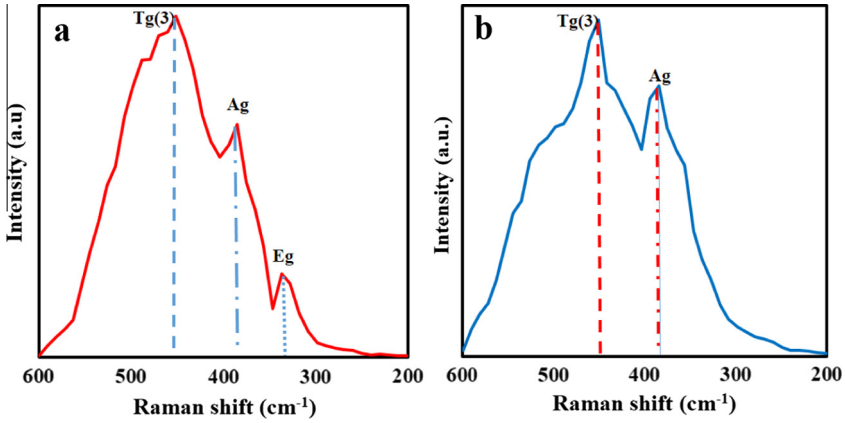

Fig. 6. Comparison of Raman spectra for Pyrite NCs, (a) Ultrasound method (10 min ultrasound irradiation, 70 °C, 70% electrical power) and (b) Classic method (24 h heating, 200 °C, reflux).

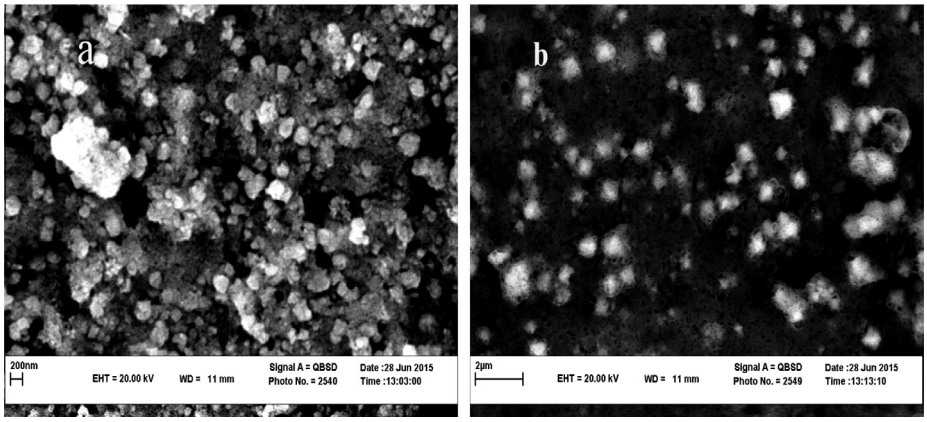

Fig. 7. SEM image (a) PU synthesized in 70 °C and 10 min with 70% amplitude by ultrasound way and (b) PC synthesized in 200 °C and 24 h by reflux way.

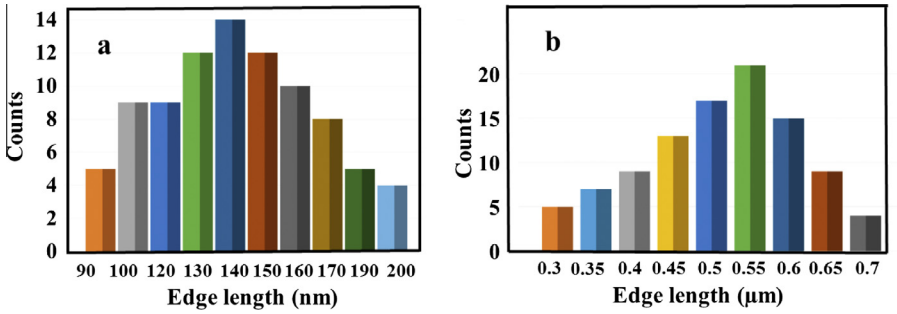

Fig. 8. Size distribution of particles by SEM images, (a) PU particles and (b) PC particles.

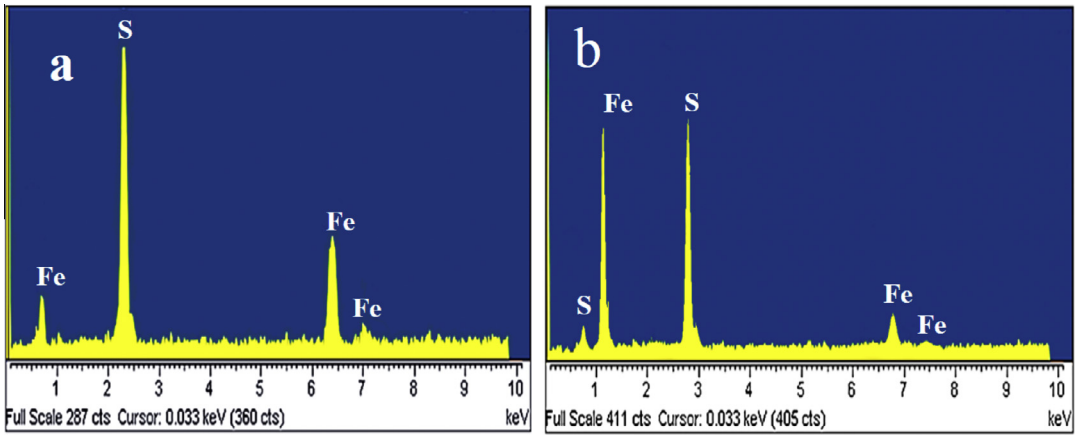

Fig. 9. EDS analysis of the synthesized pyrite (a) ultrasound method in 70 °C and 10 min with 70% amplitude and (b) classic method in 200 °C and 24 h by reflux.

for all sonication times. The comparison of FTIR spectra between PC and PU is revealed in Fig. 5. As it is clear from this figure, the functional groups of pyrite are verified in both methods.

3.5. Raman spectroscopy

The samples for Raman analysis were prepared by dispersing of NCs in water to produce a dilute suspension. Fig. 6 shows the Raman spectra for PU and PC. Ag, Eg, 3Tg, 2Au, $2E_u$ and 6Tu are the theoretical vibration modes of the pyrite and only the symmetry (gerade) vibrations (Ag, Eg, Tg(3)) are active in Raman [36,37]. Raman spectra demonstrated three bands for pyrite: dominant bands at ≈327 cm^{-1}, ≈385 cm^{-1} and a band at ≈451 cm^{-1}, which have been indexed for Eg (S_2 dumbbell stretching), Ag (in-phase stretching vibration S—S bands), and $T_g(3)$ (it is combination of stretching and vibrational signal of four adjacent S_2 units) symmetric vibrational modes, respectively. These spectra are in good agreement with previous reports [4,14,36]. The chemically ordered phase and the atomic ratio of S and Fe affect the Raman spectra. The absence of Eg peak in the classical sample can be attributed to the increase of the atomic ratio of S and Fe [45,46]. According to Fig. 6, FeS phase was not observed in both samples (lack of peaks at around 210 and 280 cm^{-1}) [47].

3.6. SEM images

The morphologies and sizes of the as-synthesized FeS_2 products were characterized by SEM. The SEM images of the typical

products obtained in the presence and absence of ultrasound are shown in (Fig. 7(a) and (b)), respectively. According to these images, the morphologies of FeS_2 products are nearly the same. The size distribution of particles that obtained from SEM images is shown in Fig. 8(a) and (b). As expected, smaller particles can be found in ultrasound sample than classical method.

3.7. EDS analysis

The chemical composition of the pyrite was more investigated by using EDS analysis. The EDS results of ultrasound and classic samples were displayed in Fig. 9. Based on the EDS analysis, only the peaks related to Fe and S elements were observed in both samples and were confirmed the purity of the products. The atomic ratios of S and Fe can be estimated to 1.46 and 1.92 for PU and PC, respectively. EDS method mostly is a qualitative method that confirmed the presence of Fe and S in both samples. EDS spectrum can be affected by various factors, the estimated lower ratio for the case of ultrasound can be attributed to the effect of ultrasound on the product.

4. Conclusion

In conclusion, FeS_2 NCs were successfully synthesized using a novel approach by utilizing ultrasonic irradiation in 10 min, 70 °C and 70% electrical power. The products were also compared with the products synthesized by the classic method. Our approach is a single-stage and does not require expensive precursors or toxic solvents and the morphologies of the products are well controlled. The high crystallinity of pyrite NCs was further confirmed by XRD. The SEM images indicated that the morphology of nanoparticles was nearly the same in the ultrasound method and the classical ones. A typical XRD pattern shows the dominant peaks which can be indexed as a pure cubic phase of FeS_2 (space group $Pa\bar{3}$) with a lattice constant of 5.418 Å in both methods, which consists with the value given in the standard card. No other impurities such as pyrrhotite, greigite are detected in both samples. XRD and EDS confirm the high purity of the sample produced under ultrasound but based on XRD pattern in classic method there was sulfur impurity. FTIR and Raman spectra proved functional groups of Fe═S, Fe—S and S—S in the samples.

Acknowledgment

The support of Ferdowsi University of Mashhad (Research and Technology) for this work (code 3/32641, date 03/02/2015) is appreciated.

References

[1] M.-L. Li, Q.-Z. Yao, G.-T. Zhou, X.-F. Qu, C.-F. Mu, S.-Q. Fu, Microwave-assisted controlled synthesis of monodisperse pyrite microspherolites, CrystEngComm 13 (2011) 5936–5942.
[2] M. Gong, A. Kirkeminde, S. Ren, Symmetry-defying iron pyrite (FeS_2) nanocrystals through oriented attachment, Sci. Rep. 3 (2013). 06/28/online 2013.
[3] D. Rickard, Pyrite: A Natural History of Fools Gold, Oxford University Press, 2015.
[4] N. Berry, M. Cheng, C.L. Perkins, M. Limpinsel, J.C. Hemminger, M. Law, Atmospheric-pressure chemical vapor deposition of iron pyrite thin films, Adv. Energy Mater. 2 (2012) 1124–1135.
[5] S. Mangham, M. Alam Khan, M. Benamara, M. Manasreh, Synthesis of iron pyrite nanocrystals utilizing trioctylphosphine oxide (TOPO) for photovoltaic devices, Mater. Lett. 97 (2013) 144–147.
[6] L. Zhu, B.J. Richardson, Q. Yu, Controlled colloidal synthesis of iron pyrite FeS_2 nanorods and quasi-cubic nanocrystal agglomerates, Nanoscale 6 (2014) 1029–1037.
[7] X. Li, W. Zhao, J. Zhao, Visible light-sensitized semiconductor photocatalytic degradation of 2,4-dichlorophenol, Sci. China, Ser. B: Chem. 45 (2002) 421–425.
[8] X. Feng, X. He, W. Pu, C. Jiang, C. Wan, Hydrothermal synthesis of FeS_2 for lithium batteries, Ionics 13 (2007) 375–377.
[9] H. Yu, E. Nie, J. Xu, S. Yan, W.J. Cooper, W. Song, Degradation of diclofenac by advanced oxidation and reduction processes: kinetic studies, degradation pathways and toxicity assessments, Water Res. 47 (2013) 1909–1918.
[10] J.C. Schlatterer, M.S. Wieder, C.D. Jones, L. Pollack, M. Brenowitz, Pyrite footprinting of RNA, Biochem. Biophys. Res. Commun. 425 (2012) 374–378.
[11] S. Fathinia, M. Fathinia, A.A. Rahmani, A. Khataee, Preparation of natural pyrite nanoparticles by high energy planetary ball milling as a nanocatalyst for heterogeneous Fenton process, Appl. Surf. Sci. 327 (2015) 190–200 (2/1/2015).
[12] P. Chin, J. Ding, J. Yi, B. Liu, Synthesis of FeS_2 and FeS nanoparticles by high-energy mechanical milling and mechanochemical processing, J. Alloy. Compd. 390 (2005) 255–260.
[13] R.J. Soukup, P. Prabukanthan, N.J. Ianno, A. Sarkar, C.A. Kamler, D.G. Sekora, Formation of pyrite (FeS_2) thin films by thermal sulfurization of dc magnetron sputtered iron, J. Vac. Sci. Technol., A 29 (2011).
[14] H.A. Macpherson, C.R. Stoldt, Iron pyrite nanocubes: size and shape considerations for photovoltaic application, ACS Nano 6 (2012) 8940–8949.
[15] S.-C. Hsiao, C.-M. Hsu, S.-Y. Chen, Y.-H. Perng, Y.-L. Chueh, L.-J. Chen, et al., Facile synthesis and characterization of high temperature phase FeS_2 pyrite nanocrystals, Mater. Lett. 75 (2012) 152–154.
[16] D.-W. Wang, Q.-H. Wang, T.-M. Wang, Controlled growth of pyrite FeS_2 crystallites by a facile surfactant-assisted solvothermal method, CrystEngComm 12 (2010) 755–761.
[17] R. Weerasooriya, B. Dharmasena, Pyrite-assisted degradation of trichloroethene (TCE), Chemosphere 42 (2001) 389–396.
[18] D. Wang, Q. Wang, T. Wang, Shape controlled growth of pyrite FeS_2 crystallites via a polymer-assisted hydrothermal route, CrystEngComm 12 (2010) 3797–3805.
[19] P. Kush, N. Mehra, S. Deka, Synthesis, characterization and optical properties of novel hierarchical flower like pyrite FeS_2 particles for low cost photovoltaics, Sci. Adv. Mater. 5 (2013) 788–795.
[20] J.M. Lucas, C.-C. Tuan, S.D. Lounis, D.K. Britt, R. Qiao, W. Yang, et al., Ligand-controlled colloidal synthesis and electronic structure characterization of cubic iron pyrite (FeS_2) nanocrystals, Chem. Mater. 25 (2013) 1615–1620.
[21] N. E'jazi, M. Aghaziarati, Determination of optimum condition to produce nanocrystalline pyrite by solvothermal synthesis method, Adv. Powder Technol. 23 (2012) 352–357.
[22] D.Y. Wang, Y.T. Jiang, C.C. Lin, S.S. Li, Y.T. Wang, C.C. Chen, et al., Solution-processable pyrite FeS_2 nanocrystals for the fabrication of heterojunction photodiodes with visible to NIR photodetection, Adv. Mater. 24 (2012) 3415–3420.
[23] S. Mohammadkhani, M. Aghaziarati, Production of iron disulfide nanoparticles by hydrothermal process, Int. J. Nanosci. Nanotechnol. 6 (2010) 231–235.
[24] R. Wu, Y. Zheng, X. Zhang, Y. Sun, J. Xu, J. Jian, Hydrothermal synthesis and crystal structure of pyrite, J. Cryst. Growth 266 (2004) 523–527.
[25] A. Gartman, G.W. Luther III, Comparison of pyrite (FeS_2) synthesis mechanisms to reproduce natural FeS_2 nanoparticles found at hydrothermal vents, Geochim. Cosmochim. Acta 120 (2013) 447–458.
[26] S. Kawai, R. Yamazaki, S. Sobue, E. Okuno, M. Ichimura, Electrochemical deposition of iron sulfide thin films and heterojunction diodes with zinc oxide, APL Mater. 2 (2014) 032110.
[27] K. Anuar, W. Tan, N. Saravanan, S. Ho, S. Gwee, Influence of pH values on chemical bath deposited FeS_2 thin films, Pacific J. Sci. Technol. 10 (2009) 801–805.
[28] K.P. Bhandari, P.J. Roland, T. Kinner, Y. Cao, H. Choi, S. Jeong, et al., Analysis and characterization of iron pyrite nanocrystals and nanocrystalline thin films derived from bromide anion synthesis, J. Mater. Chem. A 3 (2015) 6853–6861.
[29] B. Yuan, W. Luan, S.-T. Tu, J. Wu, One-step synthesis of pure pyrite FeS_2 with different morphologies in water, New J. Chem. (2015).
[30] S. Peiffer, T. Behrends, K. Hellige, P. Larese-Casanova, M. Wan, K. Pollok, Pyrite formation and mineral transformation pathways upon sulfidation of ferric hydroxides depend on mineral type and sulfide concentration, Chem. Geol. 400 (2015) 44–55.
[31] S. Khalid, E. Ahmed, M.A. Malik, D.J. Lewis, S.A. Bakar, Y. Khan, et al., Synthesis of pyrite thin films and transition metal doped pyrite thin films by aerosol-assisted chemical vapour deposition, New J. Chem. (2015).
[32] D. Wei, K. Osseo-Asare, Aqueous synthesis of finely divided pyrite particles, Colloids Surf. A: Physicochem. Eng. Aspects 121 (1997) 27–36 (3/10/1997).
[33] D. Wang, M. Wu, Q. Wang, T. Wang, J. Chen, Controlled growth of uniform nanoflakes-built pyrite FeS_2 microspheres and their electrochemical properties, Ionics 17 (2011) 163–167.
[34] M. Caban-Acevedo, D. Liang, K.S. Chew, J.P. DeGrave, N.S. Kaiser, S. Jin, Synthesis, characterization, and variable range hopping transport of pyrite (FeS_2) nanorods, nanobelts, and nanoplates, ACS Nano 7 (2013) 1731–1739.
[35] C. Janiak, T. Klapötke, H.-J. Meyer, R. Alsfasser, E. Riedel, Moderne Anorganische Chemie (2008).
[36] B. Yuan, W. Luan, S.-T. Tu, One-step synthesis of cubic FeS_2 and flower-like $FeSe_2$ particles by a solvothermal reduction process, Dalton Trans. 41 (2012) 772–776.
[37] A. Kleppe, A. Jephcoat, High-pressure Raman spectroscopic studies of FeS_2 pyrite, Mineral. Mag. 68 (2004) 433–441.
[38] K.S. Suslick, The Chemistry of Ultrasound, Encyclopaedia Britannica, Chicago, 1994, pp. 138–155.

[39] S.E. Mills, A.G. Tomkins, R.F. Weinberg, H.-R. Fan, Implications of pyrite geochemistry for gold mineralisation and remobilisation in the Jiaodong gold district, northeast China, Ore Geol. Rev. 71 (2015) 150–168.
[40] M. de Andrade Gomes, M. Ernesto Giroldo Valerio, Z. Soares Macedo, et al., Particle size control of Y_2O_3:Eu^{3+} prepared via a coconut water-assisted sol-gel method, J. Nanomater. 20 (2011) 6.
[41] R. Rath, S. Subramanian, T. Pradeep, Surface chemical studies on pyrite in the presence of polysaccharide-based flotation depressants, J. Colloid Interface Sci. 229 (2000) 82–91.
[42] F.-L. Pua, C.-H. Chia, S. Zakari, T.-K. Liew, M.A. Yarmo, N.M. Huang, Preparation of transition metal sulfide nanoparticles via hydrothermal route, Sains Malaysiana 39 (2010) 243–248.
[43] S. Middya, A. Layek, A. Dey, P.P. Ray, Synthesis of nanocrystalline FeS_2 with increased band gap for solar energy harvesting, J. Mater. Sci. Technol. 30 (8) (2014) 770–775.
[44] L. Ding, X. Fan, X. Sun, J. Du, Z. Liu, C. Tao, Direct preparation of semiconductor iron sulfide nanocrystals from natural pyrite, RSC Adv. 3 (2013) 4539–4543.
[45] G. Lucovsky, F.L. Galeener, R.C. Keezer, R. Geils, H. Six, Structural interpretation of the infrared and Raman spectra of glasses in the alloy system Ge_{1-x} S_x, Phys. Rev. B 10 (1974) 5134.
[46] K. Nakamoto, Infrared and Raman Spectra of Inorganic and Coordination Compounds, Wiley Online Library, 1986.
[47] Y. Bi, Y. Yuan, C.L. Exstrom, S.A. Darveau, J. Huang, Air stable, photosensitive, phase pure iron pyrite nanocrystal thin films for photovoltaic application, Nano Lett. 11 (2011) 4953–4957.